GPR55: A therapeutic target for Parkinson's disease?

Marta Celorrio [a, b], Estefanía Rojo-Bustamante [a, b], Diana Fernández-Suárez [a, 1],
Elena Sáez [c], Ander Estella-Hermoso de Mendoza [c], Christa E. Müller [d],
María J. Ramírez [e, g], Julen Oyarzábal [c], Rafael Franco [a, f, 2], María S. Aymerich [a, b, g, *, 2]

[a] Program of Neurosciences, Center for Applied Medical Research (CIMA), University of Navarra, Pamplona 31008, Spain
[b] Department of Biochemistry and Genetics, School of Science, University of Navarra, Pamplona 31008, Spain
[c] Small Molecule Discovery Platform, Molecular Therapeutics Program, Center for Applied Medical Research (CIMA), University of Navarra, Pamplona 31008, Spain
[d] PharmaCenter Bonn, Pharmaceutical Institute, Pharmaceutical Chemistry I, An der Immenburg 4, D-53121 Bonn, Germany
[e] Department of Pharmacology, School of Pharmacy, University of Navarra, Pamplona 31008, Spain
[f] Department of Biochemistry and Molecular Biology, University of Barcelona, Barcelona 08028, Spain
[g] IdiSNA, Navarra Institute for Health Research, Pamplona 31008, Spain

ARTICLE INFO

ABSTRACT

The GPR55 receptor is expressed abundantly in the brain, especially in the striatum, suggesting it might fulfill a role in motor function. Indeed, motor behavior is impaired in mice lacking GPR55, which also display dampened inflammatory responses. Abnormal-cannabidiol (Abn-CBD), a synthetic cannabidiol (CBD) isomer, is a GPR55 agonist that may serve as a therapeutic agent in the treatment of inflammatory diseases. In this study, we explored whether modulating GPR55 could also represent a therapeutic approach for the treatment of Parkinson's disease (PD). The distribution of GPR55 mRNA was first analyzed by in situ hybridization, localizing GPR55 transcripts to neurons in brain nuclei related to movement control, striatum, globus pallidus, subthalamic nucleus, substantia nigra and cortex. Striatal expression of GPR55 was downregulated in parkinsonian conditions. When Abn-CBD and CBD (5 mg/kg) were chronically administered to mice treated over 5 weeks with 1-methyl-4-phenyl-1,2,3,6-tetrahydropyridine and probenecid (MPTPp), Abn-CBD but not CBD prevented MPTPp induced motor impairment. Although Abn-CBD protected dopaminergic cell bodies, it failed to prevent degeneration of the terminals or preserve dopamine levels in the striatum. Both compounds induced morphological changes in microglia that were compatible with an anti-inflammatory phenotype that did not correlate with a neuroprotective activity. The symptomatic relief of Abn-CBD was further studied in the haloperidol-induced catalepsy mouse model. Abn-CBD had an anti-cataleptic effect that was reversed by CBD and PSB1216, a newly synthesized GPR55 antagonist, and indeed, two other GPR55 agonists also displayed anti-cataleptic effects (CID1792197 and CID2440433). These results demonstrate for the first time that activation of GPR55 might be beneficial in combating PD.

© 2017 Elsevier Ltd. All rights reserved.

1. Introduction

Although G-protein-coupled receptor 55 (GPR55) was considered a cannabinoid receptor, it differs phylogenetically from cannabinoid type 1 (CB$_1$) and type 2 (CB$_2$) receptors as it lacks the classic cannabinoid-binding pocket (Baker et al., 2006). GPR55 is sensitive to an array of cannabinoids (Petitet et al., 2006; Lauckner et al., 2008), although the most consistently described agonist is the endogenous lipid, lysophosphatidylinositol (LPI) (Oka et al., 2007; Henstridge et al., 2009). Despite discrepancies in downstream signaling of GPR55, a growing body of evidence points to the involvement of both G$_{12}$ and G$_{13}$ proteins that activate RhoA and mobilize Ca^{2+} (Ryberg et al., 2007; Lauckner et al., 2008; Henstridge et al., 2009), probably in an agonist- and tissue-dependent manner (Ross, 2009).

Abbreviations

6-OHDA	6-hydroxydopamine
Abn-CBD	abnormal-cannabidiol
CB_1	cannabinoid receptor type 1
CB_2	cannabinoid receptor type 2
CBD	cannabidiol
Ctx	cortex
DA	dopamine
DOPAC	3,4-Dihydroxyphenylacetic acid
GFAP	glial fibrillary acidic protein
GPe	external segment of the globus pallidus
GPR55	G-protein-coupled receptor 55
Hal	haloperidol
HPLC	High Performance Liquid Chromatography
HVA	homovanillic acid
Iba-1	ionized calcium-binding adapter molecule 1
ISH	*in situ* hybridization
IHC	immunohistochemistry
LPI	lysophosphatidylinositol
MPTP	1-methyl-4-phenyl-1,2,3,6-tetrahydropyridine
MPTPp	MPTP plus probenecid
PD	Parkinson's disease
PFA	paraformaldehyde
SN	*substantia nigra*
SNpc	*substantia nigra pars compacta*
SNpr	*substantia nigra pars reticulata*
STN	subthalamic nucleus
TH	tyrosine hydroxylase

GPR55 mRNA has been described in different regions of the mouse and human nervous system (Ryberg et al., 2007; Henstridge et al., 2011; Wu et al., 2013). GPR55 is involved in dorsal root ganglia excitability (Lauckner et al., 2008), in axon growth and in the target innervation of retinal projections during development (Cherif et al., 2015), as well as in procedural memory (Marichal-Cancino et al., 2016). The significant expression in the striatum suggests an important role of GPR55 in this region. In fact, the motor behavior of mice lacking GPR55 is impaired (Wu et al., 2013; Meadows et al., 2015; Bjursell et al., 2016). These mice also develop less severe experimental colitis (Schicho et al., 2011) and there is an absence of inflammatory response or mechanical hyperalgesia in a model of neuropathic hypersensitivity (Staton et al., 2008). Together, these data support a relevant role for this receptor in the regulation of both neural transmission and neuroinflammation.

Pharmacological studies of cannabidiol (CBD) have shown a wide range of actions in different systems and in neurodegenerative diseases (McPartland et al., 2015; Iuvone et al., 2009). In the hippocampus, CBD may prevent the pro-inflammatory glial cell activation induced by the amyloid beta administration (Esposito et al., 2007). Moreover, administration of CBD attenuates the dopaminergic system impairment that follows to a lesion with 6-hydroxydopamine (6-OHDA) in rats, that effect was attributed to the anti-inflammatory and anti-oxidant properties of CBD (Lastres-Becker et al., 2005). However, a clinical trial using a standardized plant extract containing CBD showed that the treatment, despite being well tolerated by patients with Parkinson's disease (PD), it lacked pro- or anti-parkinsonian effects (Carroll et al., 2004). Abnormal-cannabidiol (Abn-CBD) is a synthetic CBD isomer that binds to GPR55 (Johns et al., 2007; Ryberg et al., 2007; McKillop et al., 2013). This isomer has vasoactive properties (Su et al., 2015), as well as a glucose-lowering and insulinotropic capacity (McKillop et al., 2013; McKillop et al., 2016), and therapeutic potential in the treatment of inflammatory bowel diseases (Krohn et al., 2016).

Given the effect of ligands and the properties of null mutant mice, GPR55 could be a target to combat inflammation and movement disorders. Indeed, the neuroinflammatory component in PD led us to hypothesize that GPR55 could represent a therapeutic target for this neurodegenerative disease. Accordingly, we set out here to determine whether GPR55 was expressed in the brain nuclei involved in movement control that are affected in PD. As this proved to be the case, we then explored the consequences of Abn-CBD or CBD administration in the MPTP mouse model of PD. As a result, we found Abn-CBD to have a beneficial effect in this rodent model of PD, an effect that was not mediated by glial cells.

2. Materials and methods

2.1. Animals

Adult male C57BL/6 mice (25–30 g), 3 months old (Charles River, Barcelona, Spain), were housed 5 to a cage at 21 °C in a humidity-controlled environment, and on a 12 h light/dark cycle (lights on at 8 a.m.) with *ad libitum* access to food and water. All procedures involving animals were carried out in accordance with the EU Directive 2010/63/EU governing the care and use of laboratory animals. All the experimental protocols were approved by the Ethical Committee for Animal Testing of the University of Navarra (ref. 004/10).

2.2. Chronic MPTP mouse model and pharmacological treatments

To induce a bilateral, progressive and partial dopaminergic lesion, mice received 10 intraperitoneal (i.p.) injections of MPTP hydrochloride (20 mg/kg in saline: Sigma-Aldrich, St. Louis, MO, USA) plus probenecid (250 mg/kg in saline: Invitrogen, Paisley, UK), administered twice a week over 5 weeks (Fig. 1). Probenecid reduces the renal clearance of MPTP and its metabolites, provoking a sustained toxic response (Lau et al., 1990). MPTP and probenecid (MPTPp) were administered in two consecutive injections, while the control groups of animals received probenecid and saline (Braun, Barcelona, Spain) on an identical administration regime at 9 a.m.. Animals were divided into 6 groups for the pharmacological treatments, 3 MPTPp and 3 control groups. The 3 groups of MPTPp
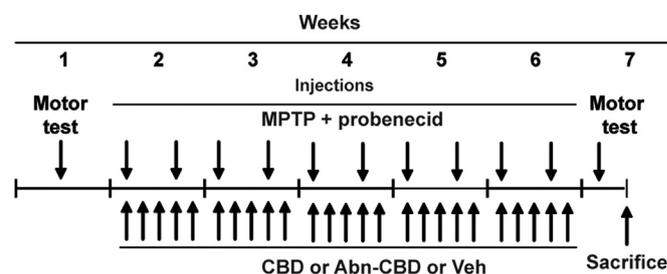
Fig. 1. Schedule of MPTP, probenecid, CBD and Abn-CBD administration. Control animals were treated with saline, probenecid (250 mg/kg) and either CBD (5 mg/kg), Abn-CBD (5 mg/kg) or the vehicle used to prepare the compounds. MPTPp animals were injected with MPTP (20 mg/kg) and probenecid (250 mg/kg) and either CBD, Abn-CBD or the vehicle alone. Parkinsonian motor symptoms were evaluated 24 h after the last MPTPp injection (16 h after the last Abn-CBD administration); animals were sacrificed at 48 h (40 h after the last Abn-CBD administration).

mice received either cannabidiol (CBD, 5 mg/kg: Tocris, Bristol, UK), abnormal-cannabidiol (Abn-CBD, 5 mg/kg: Tocris) or just the vehicle in which these drugs were dissolved, saline containing 15% dimethylsulfoxide (DMSO, Sigma-Aldrich), 5% polyethylene glycol (PEG, Sigma-Aldrich) and 5% Tween-80 (Guinama, Valencia, Spain). The 3 groups of control mice also received CBD, Abn-CBD or the vehicle alone. CBD and Abn-CBD were administered i.p. 5 days a week over 5 weeks at 5 p.m., and the mice were sacrificed 48 h after the last MPTPp administration (40 h after the last administration of CBD and Abn-CBD/vehicle).

2.3. Haloperidol-induced catalepsy mouse model

Catalepsy was induced in naïve animals with an i.p. injection of haloperidol (Hal, 1 mg/kg: Sigma-Aldrich) dissolved in 1.3% DMSO and 1.3% Tween-80. Two hours later, different drugs were administered (i.p.): SCH442416 (1 mg/kg: Tocris), an adenosine receptor subtype 2 (A_{2A}) antagonist used as a positive anti-cataleptic control; CBD (5 mg/kg and 20 mg/kg: Tocris); Abn-CBD (20 mg/kg: Tocris); PSB1216 (10 mg/kg: Bonn Unversität, Bonn, Germany), a GPR55 antagonist; CID85469571 (20 mg/kg: Aobious, Gloucester, MA, USA), a GPR18 antagonist; CID1792197 (10 mg/kg) and CID2440433 (40 mg/kg), GPR55 agonists; Rimonabant (3 mg/kg: Cayman, Ann Arbor, MI, USA), a CB_1 antagonist; AM630 (3 mg/kg: Tocris), a CB_2 antagonist; and WIN55,212-2 (3 mg/kg: Tocris), a CB_1 and CB_2 receptor agonist The cataleptic status of mice was evaluated in the bar test 60 min later (180 min after hal injection).

2.4. Behavioral tests

The behavioral tests on the MPTPp mice were performed under low light conditions 24 h after the last MPTP and probenecid injection, and 16 h after the last CBD or Abn-CBD (or vehicle) administration. In the rotarod assay (LE8200, Panlab, Barcelona, Spain), the animals were placed on the rod and the rotarod was programmed to rotate at a speed that increased linearly from 4 to 40 rpm over 5 min. The time each mouse remained on the rod was recorded up to a maximum of 5 min. All animals were pre-trained until they were able to remain on the rod for at least 60 s prior to MPTPp intoxication. The average permanence was calculated from 3 consecutive trials with a resting time of 30 min between each of them. For the pole test, the animals were placed with their head facing upwards on the top of a 50 cm high and 1 cm diameter, vertical wooden pole covered with a bandage. Prior to MPTPp intoxication, all the animals were pre-trained until they were able to reverse their position and descend the pole in less than 5 s. The animal's movement was recorded and all the videos were analyzed blind to the experimental conditions. The average time taken to turn their head and descend the entire pole was measured in 3 trials with a resting time of 30 min between each of them. Cataleptic status was evaluated using the bar test 60 min after the administration of compounds. Animals were placed with their forepaws on a cylindrical metal bar oriented parallel to the ground at a height of 4 cm. The time elapsed before the animals moved from this position was the parameter measured, with a maximum permitted time of 1 min on the bar per trial.

2.5. Tissue processing

Animals were sacrificed by cervical dislocation for biochemical studies or by transcardial perfusion for histological analysis. For biochemical studies, their brain was removed rapidly, frozen on dry ice and stored at −80 °C. For histological techniques, mice were anesthetized with 10% chloral hydrate (Sigma-Aldrich) and perfused transcardially with 4% paraformaldehyde (PFA, Merck,

Darmstadt, Germany) in 0.125 M phosphate buffered saline (PBS, pH 7.4). Their brain was then removed and cryoprotected for 48 h in 20% glycerol and 2% DMSO in PBS.

2.6. Dopamine quantification

Striatal concentrations of dopamine (DA), 3,4-dihydroxyphenylacetic acid (DOPAC) and homovanillic acid (HVA) were determined by high performance liquid chromatography (HPLC) with electrochemical detection, as described previously (Goñi-Allo et al., 2006). Briefly, samples were injected using an automatic sample injector (Waters 717 plus, Waters Cromatografía, S.A., Barcelona, Spain) onto a Spherisorb ODS-2 reverse phase C^{18} column (5 m, 150 × 4.6 mm: Teknokroma, Barcelona, Spain) connected to a DECADE amperometric detector (Antec Leyden, Zoeterwoude, the Netherlands), with a glassy carbon electrode maintained at 0.7 V with respect to a Ag/AgCl reference electrode. The mobile phase consisted of 0.1 M citric acid, 0.1 M Na_2HPO_4, 0.74 mM octanesulphonic acid, 1 mM EDTA and 16% methanol (pH 3.4), pumped at a flow rate of 1 mL/min.

2.7. Determination of brain to plasma concentration ratio at Tmax

In order to obtain the brain to plasma (B/P) ratio, Abn-CBD was injected (20 mg/kg, i.p.) to mice (n = 5), 3 control mice received the Abn-CBD vehicle. Animals were sacrificed by cervical dislocation 60 min later. Brains were homogenized in PBS (670 μL/g of tissue) using a Branson 250 ultrasonic probe sonicator (Branson, Danbury, Connecticut, USA). Plasma samples (10 μL) and brain homogenate equivalent to 75 mg of tissue were used. Chromatographic separation was performed by gradient elution at 0.6 mL/min using an Acquity UPLC BEH C^{18} column (50 × 2.1 mm, 1.7 μm particle size; Waters). The mobile phase consisted of A: 0.1% formic acid in water, B: 0.1% formic acid in methanol. The autosampler temperature was set at 10 °C and column temperature at 40 °C. For detection and quantification, the electrospray ionization operated in the positive mode was set up for multiple reaction monitoring (MRM). The collision gas used was ultra-pure argon at a flow rate of 0.15 mL/min. Quantification was achieved by external calibration using matrix-matched standards. Concentrations were calculated using a weighted least-squares linear regression (W = 1/x). Calibration standards were prepared by adding the appropriate volume of diluted solutions of the compound in a mixture of methanol and water (50:50, v:v) to aliquots of 10 μL of plasma or tissue homogenate. To precipitate proteins of the standards and samples, 200 μL of 3% formic acid in methanol containing 50 nM tolbutamide (used as internal standard) were added. The mixture was then agitated for 5 min and centrifuged at 13,200 rpm for 10 min at 4 °C. A 3 μL aliquot of the supernatant was injected into the LC-MS/MS system for analysis.

2.8. RNA extraction and qPCR

Total RNA from striatal samples was extracted using Trizol (Invitrogen) and DNase I. Reverse transcription of total RNA (2 μg) was performed with 200 U M-MLV reverse transcriptase (Promega) and 2.5 mM random hexamer oligodeoxyribonucleotides (Invitrogen). Messenger RNA (mRNA) expression was assessed by real-time polymerase chain reaction (RT-PCR) in a CFX96 real-time system, using 0.5x of the IQ SYBR Green Mix (BioRad Laboratories, Alcobendas, Madrid, Spain) and 0.3 μM of the specific primers for the mice cannabinoid GPR55 receptor: sense-ATCTTTGGCTTCCTCCTTCC and antisense-CCCTTAGTGTCTCTCTGTTG diluted to a total volume of 10 μL by adding sterile H_2O. The data were normalized to GAPDH and the

amount of each transcript was expressed as 2ΔCt (ΔCt = Ct [GAPDH] - Ct [gene]), with Ct as the point at which the fluorescent signal rose significantly above the background fluorescence.

2.9. Immunohistochemistry

Immunohistochemistry (IHC) was performed on free-floating sections (40 μm thick) and in a given experiment, all the sections were processed at the same time with each primary antibody. Sections were washed with PBS and endogenous peroxidase activity was inactivated by incubating them for 30 min with 0.03% H_2O_2 (Sigma-Aldrich) in methanol (Panreac, Barcelona, Spain). After washing 3 times with PBS, the tissue was incubated for 40 min with blocking solution [4% normal goat serum, 0.05% Triton X-100 (Sigma-Aldrich) and 4% bovine serum albumin (BSA, Merck, Darmstadt, Germany) in PBS], and it was exposed overnight at room temperature (RT) to the primary antibodies diluted in blocking solution. The primary antibodies used for colorimetric IHC were: rabbit anti-tyrosine hydroxylase (TH, 1:1000: Millipore, Temecula, CA, USA), rabbit anti-glial fibrillary acidic protein (GFAP, 1:500: Dako, Glostrup, Denmark) and rabbit anti-ionized calcium-binding adapter molecule 1 (Iba1, 1:500: Wako, Osaka, Japan). Antibody binding was detected by incubating the sections for 2 h at RT with a biotinylated goat anti-rabbit secondary antibody (1:1000: Jackson ImmunoResearch Laboratories, West Gore, PA, USA) diluted in blocking solution. The biotinylated antibodies were detected by incubating for 90 min at RT with peroxidase-conjugated avidin (1:5000: Sigma-Aldrich) followed by incubation with 0.05% diaminobenzidine (DAB, Sigma-Aldrich) in 0.03% H_2O_2/Trizma-HCl buffer [pH 7.6]. The primary antibodies used for fluorescence IHC were: goat anti-tyrosine hydrolase (TH, 1:50: Santa Cruz Biotechnology), mouse anti-neuronal nuclear antigen (NeuN, 1:1000: Millipore, Temecula, CA), rabbit anti-GFAP (1:500), and rabbit anti-Iba1 (1:500). The primary antibodies were detected with Alexa-633 donkey anti-goat (1:1000: Invitrogen, Madrid, Spain), Alexa-488 donkey anti-rabbit (1:1000: Invitrogen) or Alexa-647 donkey anti-mouse (1:1000: Invitrogen), diluted in blocking solution and incubated with the sections for 2 h at RT. Sections were mounted on glass slides in a 0.2% solution of gelatin in 0.05 M Tris-HCl buffer [pH 7.6] (Sigma-Aldrich), and they were dried and dehydrated in toluene (Panreac) for 12 min before coverslipping with DPX (BDH Chemicals, Poole, UK).

2.10. In situ hybridization

The riboprobe to detect GPR55 was synthesized from cDNA retrotranscribed from total RNA isolated from a C57BL/6 adult male mouse spleen. Specific primers for GPR55 were designed using Primer3 Input v.0.4.0 software (http://frodo.wi.mit.edu/cgi-bin/primer3/primer3_www.cgi): sense, TCACCATCTGCTTCATCAGC and antisense, CCTGGTTGACCAGCTTGATT. PCR was performed by adding 4 U Bio X Short DNA Polymerase (Bioline USA Inc, Tauton, MA, USA), 200 μM dNTPs, 0.1 M $MgCl_2$, 0.1 μM forward primer, 0.1 μM reverse primer and 1.5 μg of cDNA, and bringing the mix to a total volume of 50 μL by adding sterile H_2O. After an initial denaturation at 95 °C for 5 min, 35 amplification cycles (denaturation at 95 °C for 60 s, annealing at 56 °C for 60 s and extension at 68 °C for 60 s) and a final extension for 10 min at 72 °C were performed. The PCR product was then inserted into a plasmid vector (PCR® II-TOPO®; Invitrogen), and used to transform competent E. Coli (Invitrogen) by adding 5 μL of the ligation reaction a 50 μL vial of competent cells and mixing by tapping gently. The cells were incubated on ice for 30 min, incubated at 42 °C for 30 s and then placed on ice. Pre-warmed super optimal broth (SOC, Invitrogen) was added to the cells (250 μL) and the vials were shaken for 1 h at

225 rpm in a rotary shaker-incubator set to 37 °C. The transformed cells were then spread on LB agar plates and incubated at 37 °C overnight. DNA was then isolated from selected colonies using QIAprep Spin Miniprep kit (Invitrogen) and the purified DNA was sequenced on an ABI 3130 Genetic Analyzer (Applied Biosystems, Invitrogen) using T7 and SP6 primers, and a BigDye Terminator V3.1 cycle sequencing kit (Applied Biosystems, Invitrogen). The plasmid (13 μg) was then linearized with the Xba1 restriction enzyme (20 U: New England Biolabs, Ipswich, MA) to obtain the sense probe, or with SpeI (10 U: New England Biolabs) to obtain the antisense probe. The linearized plasmids were transcribed with the appropriate RNA polymerases (Roche, Basel, Switzerland), in a 20 μL transcription mixture that included 2 μg template plasmid, 1x digoxigenin-NTP (Roche), 20 U RNase inhibitor (Invitrogen) and 40 U of the T7 or SP6 RNA polymerase (Roche). After a 2 h incubation at 37 °C, the template plasmid was digested with 10 U RNase-free DNase (Roche) for 30 min at 37 °C. The enzymes and proteins were digested with 0.025 μg/μL proteinase K (Roche) for 15 min at 55 °C, and the enzymes were then denatured for 5 min at 90 °C. The sense and antisense riboprobes were then precipitated by the addition of 0.05 M ammonium acetate and ethanol, and they were recovered by centrifugation at 4 °C for 30 min. The pellet was washed with 70% ethanol, centrifuged at 13,000xg at 4 °C for 30 min, dissolved in 30 μL H_2O-DEPC and stored at −80 °C.

Colorimetric *in situ* hybridization (ISH) was performed on free-floating sections incubated in 0.1% active H_2O-DEPC in 0.125 M PBS for 5 min. After pre-equilibration in 5x SSC (0.75 M NaCl, 7.5 mM Na-citrate) for 10 min, the sections were pre-hybridized for 2 h at 58 °C in the hybridization solution (50% deionized formamide [Sigma-Aldrich], 5x SSC and 40 μg/mL of denatured salmon DNA [Sigma-Aldrich] in H_2O-DEPC). The digoxigenin labeled probes (Roche) were denatured for 15 min at 75 °C and added to the hybridization mix at a concentration of 400 ng/mL, hybridizing the sections in this solution for 16 h at 58 °C. The sections were then washed three times in 2x SSC at RT for 5 min, in 2x SSC at 65 °C for 1 h and then in 0.1x SSC at 65 °C for 1 h. Subsequently, the sections were immersed for 30 min in 0.03% H_2O_2 in order to inactivate the endogenous peroxidase activity and they were then pre-equilibrated in TN buffer (0.1 M Tris-HCl pH 7.5, 0.15 M NaCl), prior to incubating them for 2 h at RT with the alkaline-phosphatase-conjugated anti-digoxigenin antibody fab fragments raised in sheep (1:1000; Roche) in 0.5% TN-blocking reagent (0.5 g of Blocking Reagent [Roche] in 100 mL of TN buffer). After several rinses in TN buffer, the sections first were equilibrated for 5 min in TNM buffer (0.1 M Tris−HCl, 0.1 M NaCl, 0.05 M $MgCl_2$ [pH 9.5]) and then incubated for 7 h in a substrate solution (0.02% of nitro blue tetrazolium −NBT- [Roche] with 5-bromo-4-chloro-3-indolylphosphate −BCIP- [Roche] in TNM buffer). Staining was terminated by washing several times in PBS and the sections were finally mounted on slides, air-dried, dehydrated in alcohol, cleared in xylene and coverslipped with Entellan (Merck).

The protocol for fluorescent ISH was similar to the colorimetric procedure except that the anti-digoxigenin antibody was visualized using 2-hydroxy-3-naphtoic acid-2′-phenylanilide phosphate (HNPP fluorescence detection kit, Sigma-Aldrich) following the manufacturer's instructions. For co-localization experiments, the fluorescence IHC was commenced after washing out the HNPP solution.

2.11. Image analysis

For a given experiment, immunostaining of the different samples was performed simultaneously and the images were captured using the same parameters. Colorimetric images were digitized in a grey scale under constant light conditions using a DXM1200F

digital camera coupled to an Eclipse microscope (Nikon, Barcelona, Spain). Sections were captured at 20X magnification and in each section, two portions (580 μm x 424 μm) of the left and the right striatum, 0.38 mm from Bregma, according to the Mouse Brain Atlas (Paxinos and Franklin, 2001) were analyzed blindly using Metamorph image analysis software (Molecular Devices, Sunnyvale, CA). A fixed threshold was applied to all images and the percentage of pixels detected was automatically calculated for each image.

Confocal images from control and MPTPp mice of the GPR55 receptor detected by ISH in combination with IHC for NeuN in the striatum and TH in the SNpc, were acquired on an LSM 510 confocal microscope (Zeiss) using a 40X oil objective. A projection stack of 10 images per slice was analyzed using Metamorph image analysis software (Molecular Devices, Sunnyvale, CA). A region on interest (ROI) comprising the NeuN-immunopositive neurons in the striatum or the TH-immunopositive neurons in the SNpc was delineated. A fixed threshold was then applied, and the optical density of the GPR55 signal was determined from each image.

2.12. Stereological analysis

The number of TH immunolabeled neurons present in the *substantia nigra pars compacta* (SNpc) was determined by unbiased design-based stereology. Stereological counting was performed on 6 coronal SNpc sections (40 μm thick) taken at uniform intervals (120 μm) that covered the entire rostrocaudal extent of the nucleus, between −2.92 mm and −3.64 mm relative to Bregma (Paxinos and Franklin, 2001). The reference volume of the SNpc was calculated from images obtained with a 2X objective using a point count array according to Cavalieri principles (Gundersen and Jensen, 1987). The cross-sectional area of the nucleus was measured and the reference volume (Vr) for the entire SNpc was estimated using the following equation:

$$Vr = T\frac{a}{p}\sum Pi$$

where T is the section thickness, a/p is the area of each point and Pi is the number of points falling within the SNpc. Stereological counting was performed with newCAST Visiopharm software (Hoersholm) on images acquired with a Bx61 microscope (Olympus) equipped with a DP71 camera (Olympus) and a stage connected to an xyz stepper (H101BX, PRIOR). The SNpc was outlined at low magnification (4X) to estimate the area. The number of labeled neurons was calculated at 100X magnification under oil immersion, using randomized meander sampling and optical dissector methods. The optical dissector height was set at 11 μm to count 100–150 cells per animal using a sampling frame of 5294 μm^2 and sampling steps of 145 μm × 145 μm (dx, dy). Unbiased counting was performed blindly and the total number of TH-positive neurons (N) was calculated using the following formula:

$$N = \sum \mathscr{Q}^- \frac{t}{h}\frac{1}{asf}\frac{1}{ssf}$$

where $\sum Q$- is the total number of particles counted, t is the mean section thickness, h is the height of the optical dissector, asf is the area sampling fraction, and ssf is the section sampling fraction. Neuronal density (D) was determined using the following formula: D = N/Vr.

The following parameters were estimated by unbiased stereology in striatal Iba1 immunolabeled cells: neuronal density, soma area, and the length of microglial processes. This stereological analysis was performed on 5 coronal striatal sections taken between +1.34 mm and −0.26 mm relative to Bregma (Paxinos and Franklin, 2001). Approximately 100–150 cells per animal were counted using a sampling frame of 4538 μm^2 and sampling steps of 426 μm × 426 μm (dx, dy). The soma area was estimated with a 2D nucleator (Visiopharm). The total length of neurites was estimated by global spatial sampling and by counting intersections of fibers with isotropically oriented virtual planes within a virtual box in a thick section with arbitrary orientation. The total fiber length (L) was calculated as indicated elsewhere (Larsen et al., 1998).

$$L = \frac{1}{hsf}\frac{1}{asf}\frac{1}{ssf}\,d\,x\,2\,x\sum \mathscr{Q}^-$$

where d is the plane separation distance and $\sum Q$-is the total number of fiber-plane intersections counted (hsf, asf and ssf). Counting was performed at a height of 10 μm using a frame area of 227 μm^2, sampling steps of 389 μm × 389 μm (dx, dy) and a plane separation distance (d) of 20 μm (Drøjdahl et al., 2010).

2.13. Permeability assay

The permeability of compounds was evaluated using the parallel artificial membrane permeation assay (PAMPA) as an in vitro model of passive diffusion. Donor solutions of the test compounds (180 μL, 50 μM in PBS/EtOH 70:30) were added to each well of the donor plate, whose PVDF membrane was precoated with 4 μL of a 20 mg × mL^{-1} PBL/dodecane mixture. PBS/EtOH (180 μL) was added to each well of the acceptor plate, and the donor and acceptor plates were combined together and incubated for 18 h at 20 °C without shaking. In each plate, compounds and controls were tested in duplicate. Drug concentrations in the acceptor, donor and the reference wells was determined using the UV plate reader with 130 μL of the acceptor and donor samples. Permeability rates (Pe in nm s^{-1}) were calculated using Equation (1) and the permeability rate of each compound was the averaged value of three independent measurements.

$$P_e = C \times \left(-ln\left(1 - \frac{[drug]_{acceptor}}{[drug]_{equilibrium}}\right)\right) \times 10^7 ; \tag{1}$$

where $C = \frac{V_{D\times}V_A}{(V_D + V_A)\times Area \times time}$; V$_D$ = 0.18 mL; V$_A$ = 0.18 mL; Area = 0.32 cm^2; time = 64800 s; D$_F$ = 180/130; [drug]$_{equilibrium}$ = ([drug]$_{donor}$ x V$_D$ + [drug]$_{acceptor}$ x V$_A$)/(V$_D$ + V$_A$); [drug]$_{donor}$ = (A$_a$/A$_i$*D$_F$)$_{donor}$; [drug]$_{acceptor}$ = (A$_a$/A$_i$*D$_F$)$_{acceptor}$; A$_{a\ donor}$ = Abs$_{donor}$ − Abs$_{vehicle}$; A$_{a\ acceptor}$ = Abs$_{acceptor}$ − Abs$_{vehicle}$, Ai = Abs$_{withoutPBL}$ - Abs$_{vehicle}$.

2.14. Statistical analysis

The data are presented as the means ± SEM. Normality was assessed with the Kolmogorov−Smirnov test and the data following a normal distribution were analyzed by one-way ANOVA followed by Tukey's multiple comparisons test, by a two-way ANOVA followed by a Bonferroni's post-hoc test or by a *t*-test. Significant differences of the data that did not follow a normal distribution were evaluated using the Mann-Whitney test. The data were analyzed using GraphPad Prism 5 (La Jolla, CA, USA) and in all instances, p values < 0.05 were considered as statistically significant.

3. Results

3.1. GPR55 mRNA expression in the basal ganglia

GPR55 expression has previously been studied in the mouse

brain by performing PCR on tissue from the cortex, forebrain, striatum, hippocampus and cerebellum (Wu et al., 2013). Here, we assessed GPR55 mRNA expression in brain regions involved in PD by ISH, using the mouse sequence as a template to synthesize 636 base pair long, digoxigenin labeled antisense and sense riboprobes. Single colorimetric ISH with the anti-sense riboprobe showed expression of GPR55 transcripts in the cortex, striatum, external segment of the globus pallidus (GPe), subthalamic nucleus (STN) and *substantia nigra* (SN) of control mice (Fig. 2A). The GPe and the STN presented the strongest signal, with the cortex, the striatum and the SNpc displaying moderate staining, which was more intense than the signal in the SN *pars reticulata* (SNpr). ISH with the sense riboprobe produced no staining. To determine the cellular distribution of the GPR55 transcripts, dual fluorescent ISH for GPR55 and fluorescent IHC for different markers was performed in the striatum (Fig. 2B). As such, the labeling of GPR55 transcripts co-localized with that for NeuN but not with that for Iba1 or GFAP (Fig. 2B), indicating that this receptor is expressed in neurons.

The chronic MPTP mouse model was chosen as a model for PD due to the partial, bilateral and progressive dopaminergic loss that may be induced after the administration over 5 weeks of MPTP and probenecid (MPTPp; Petroske et al., 2001). The expression of GPR55 was studied in the striatum (Fig. 3A, C, D and E) and in the SNpc (Fig. 3B, F, G and H) of MPTPp and control animals. GPR55 transcripts were detected by fluorescent ISH, a specific labeling was observed in NeuN immunolabeled striatal cells (Fig. 3A). Densitometry of the fluorescent signal indicated there was significantly weaker GPR55 expression in the MPTPp mice than in the control mice (Fig. 3C). When fresh tissue was obtained from a different subset of animals to extract RNA and quantify the striatal expression of GPR55 mRNA by RT-PCR, the weaker expression in MPTPp mice was confirmed (Fig. 3D). Dual labeling to detect GPR55 by ISH and TH by IHC was performed in the SNpc indicating that dopaminergic neurons expressed GPR55 (Fig. 3E). TH-immunopositive cells express GPR55 (Fig. 3B). The densitometric analysis of GPR55 expression in neurons that co-expressed TH revealed no changes in naïve and MPTPp mice (Fig. 3F and G), although there was a clear loss of TH-positive neurons in the MPTPp animals. RT-PCR analysis of fresh tissue from the midbrain showed a significant decrease in GPR55 mRNA expression in MPTPp animals (Fig. 3H), probably due to the loss of dopaminergic cells in this region. These results demonstrate that the expression of GPR55 is differentially regulated in neurons of different brain areas under pathological conditions. GPR55 expression in the MPTPp model of PD was downregulated in the striatum but not in dopaminergic neurons of the SNpc.

3.2. The effect of chronic CBD and Abn-CBD treatment in the chronic MPTPp mouse model

To study the pharmacological effect of targeting GPR55, Abn-CBD (a CBD isomer) was selected as a GPR55 agonist (Baker et al., 2006). CBD was also used for comparative purposes. The compounds (or vehicle) were administered to the naïve or MPTPp mice 5 days a week for 5 weeks, starting on the same day of the first MPTPp injection (Fig. 1). MPTPp was administered at 9 a.m. and the drugs at 5 p.m. Motor behavior was evaluated 24 h after the last injection of MPTP and 16 h after the last injection of the test compounds. In the pole test (Fig. 4A), two-way ANOVA demonstrated a significant interaction between the lesion and the treatments ($F_{2,67} = 5.4$, $p = 0.007$). In fact, MPTPp animals treated with Abn-CBD performed significantly better than untreated MPTPp mice, while CBD did not produce a significant effect in this test. As expected, neither CBD nor Abn-CBD administration to control mice

affected their performance in the pole test. In the rotarod test (Fig. 4B), two-way ANOVA also demonstrated a significant interaction between the lesion and the treatment ($F_{2,67} = 7.2$, $p = 0.001$). While MPTPp administration significantly reduced the time mice were able to remain on the rotarod relative to the naïve animals, Abn-CBD treatment significantly increased the time MPTPp mice stayed on the rod, while it had no effect on the performance of control animals. By contrast, CBD did not have any effect in MPTPp mice whereas it significantly reduced the time on the rod of naïve animals. These results show that only chronic administration of Abn-CBD improved the motor behavior of MPTPp mice.

A neuroprotective effect of Abn-CBD could be responsible for the improvement in the motor performance of MPTPp mice. To assess the integrity of neurons in the nigrostriatal pathway, the presence of TH-positive terminals was evaluated by TH IHC in the striatum of MPTPp mice (Fig. 5A). The optical density of TH-immunolabeled striatal terminals was quantified and two-way ANOVA revealed a significant interaction between the lesion and the treatments ($F_{2,25} = 3.6$, $p = 0.04$; Fig. 5B). The density of TH-immunolabeled terminals was significantly lower in MPTPp animals and while it was not affected by the chronic administration of Abn-CBD, it was further diminished by treatment with CBD. The number of TH-labeled neurons in the SNpc (Fig. 5C) was quantified by unbiased stereology and again, two-way ANOVA of the stereological data demonstrated a significant interaction between the lesion and treatments ($F_{2,25} = 4.9$, $p = 0.02$; Fig. 5D). The number of TH-immunolabeled neurons was significantly lower in MPTPp mice that received the vehicle but it increased following Abn-CBD treatment. In accordance with the behavioral data, CBD administration did not afford any neuroprotection to these PD model animals (Fig. 5D). Together, these results suggest that chronic administration of Abn-CBD to MPTPp mice exerted a protective effect that was restricted to dopaminergic neuron cell bodies. By contrast, CBD did not display any protective effect on either cell bodies or dopaminergic terminals.

The status of glial cells was analyzed by IHC in the striatum of these animals using an antibody against Iba1, a specific microglial marker (Fig. 6A). Morphological changes in microglia that reflect different degrees of activation were studied by unbiased stereology, analyzing three parameters: cell density (Fig. 6B), cell body area (Fig. 6C), and the length of the ramifications (Fig. 6D). Although MPTPp administration only produced significant changes in the cell body area (Fig. 6C), CBD and Abn-CBD administration to MPTPp animals produced a significant decrease in the microglial cell density (Fig. 6B), in the cell body area (Fig. 6C) and in the length of microglial ramifications (Fig. 6D). Hence, unlike the behavioral assays, both CBD and Abn-CBD had a similar effect on the gross phenotypic parameters of microglia. IHC for GFAP, a marker of astroglia, revealed weak GFAP labeling in the striatum of control animals, which was enhanced similarly in MPTPp mice and in the MPTPp mice that received CBD or Abn-CBD (Figs. S1A and S1B). Thus, it appeared that these drugs had no effect on astroglial activation.

To address the possibility that Abn-CBD could upregulate DA levels in the remaining striatal dopaminergic terminals, the striatal levels of DA and its metabolites were quantified by HPLC. One-way ANOVA demonstrated that DA ($F_{2,19} = 207$; $p < 0.001$; Fig. 7A), DOPAC ($F_{2,19} = 30$; $p < 0.001$; Fig. 7B) and HVA ($F_{2,19} = 21$; $p < 0.001$; Fig. 7C) levels are significantly dampened in MPTPp mice and that they were not affected by Abn-CBD treatment. These results indicate that the improved motor behavior of MPTPp mice produced by chronic administration of Abn-CBD but not CBD is not associated to an increase in DA, nor it is mediated by protection of dopaminergic neurons in the nigrostriatal pathway.
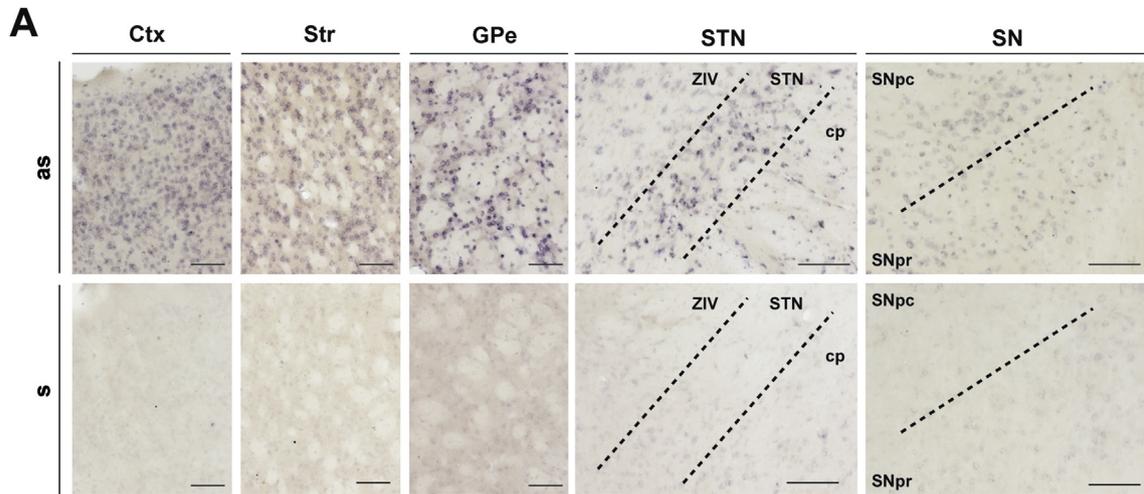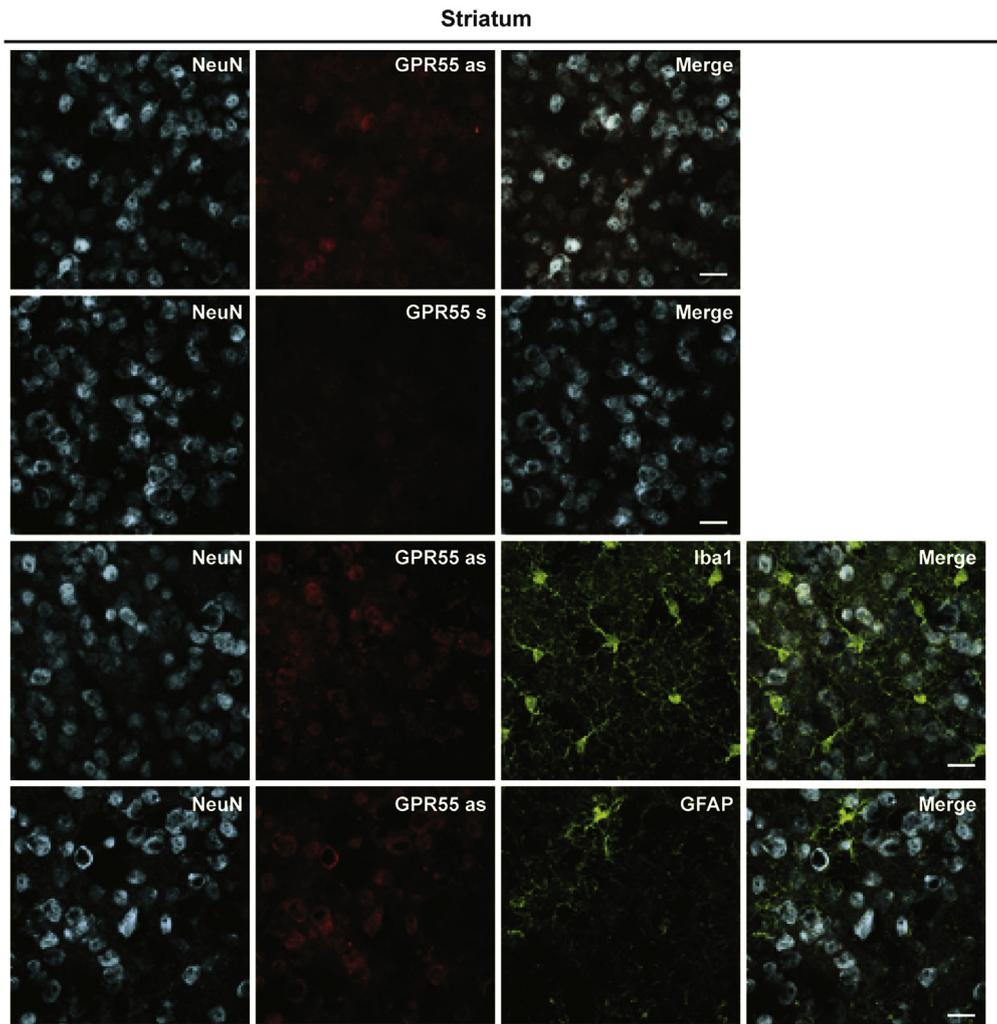
Fig. 2. *In situ* hybridization (ISH) to detect GPR55 mRNA expression in the mouse brain. (A) Single colorimetric ISH showing the expression of GPR55 in the cortex (Ctx), striatum (Str), external segment of the globus pallidus (GPe), subthalamic nucleus (STN), *substantia nigra pars compacta* (SNpc) and *substantia nigra pars reticulata* (SNpr). Hybridization with the antisense riboprobe resulted in specific labeling (upper panel) while hybridization with the sense riboprobe produced no signal (lower panel). (B) Striatal double labeling for GPR55 (by ISH) and either a neuronal (NeuN), or microglial (Iba1) or astroglial (GFAP) markers (by IHC). Scale bar: (A) 0.1 mm, (B) 20 μm. ZIV, zona incerta ventral part; cp, cerebral peduncle.
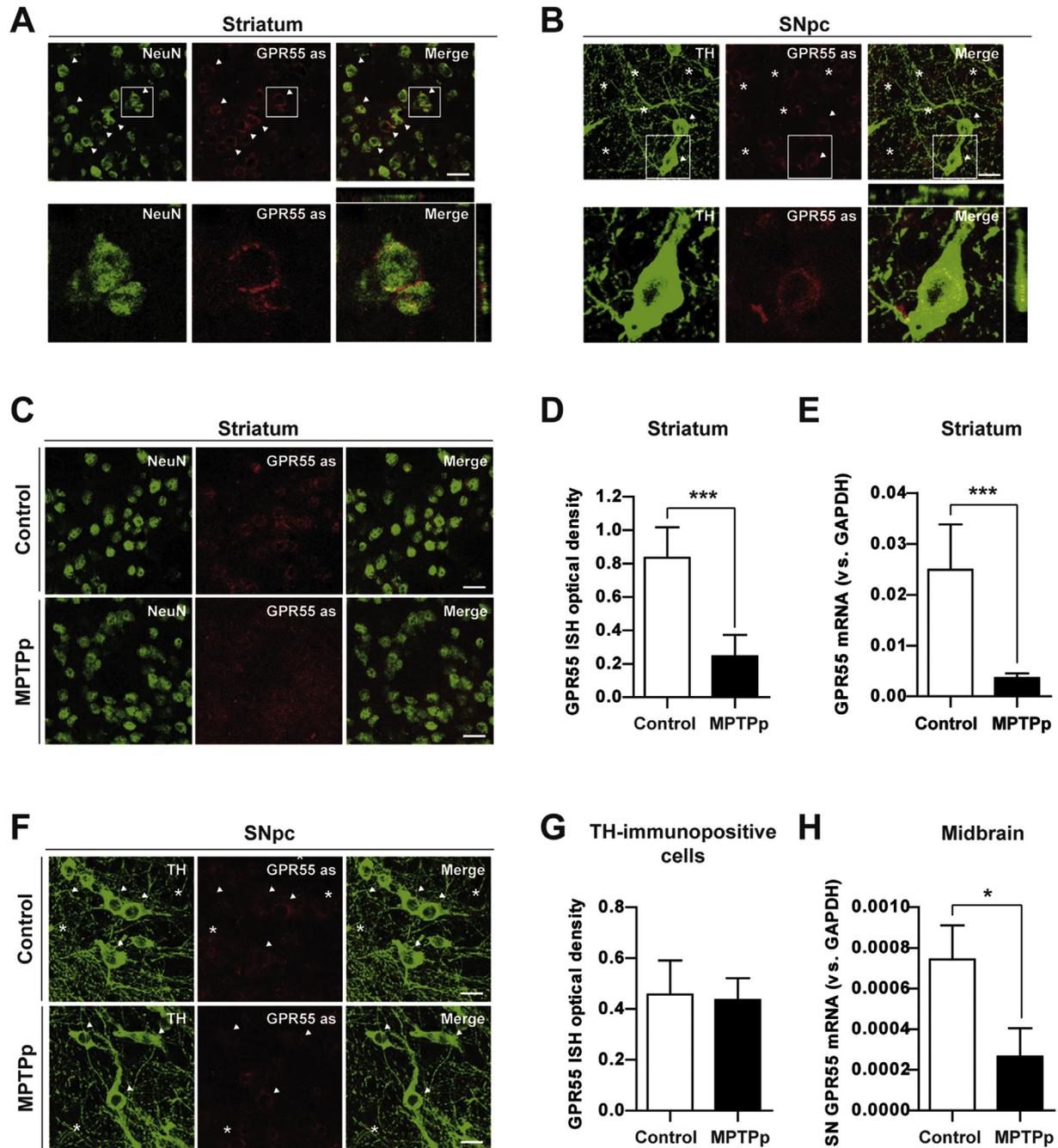
Fig. 3. GPR55 expression in the nigrostriatal pathway of control and MPTPp mice. (A) Representative confocal images were obtained from the striatum of control mice stained with NeuN and the GPR55 antisense riboprobe. Arrowheads (upper panel) indicate some representative neurons co-labeled with the neuronal nuclear marker (NeuN) and with the GPR55 riboprobe in the cytoplasm. An enlarged image is shown in the lower panel, the orthogonal projection of the Z-stack shows the NeuN nuclear staining adjacent to the GPR55 cytoplasmic expression in the same cell. (B) Representative confocal images obtained from the SNpc stained with the dopamine neuron marker (TH) and the GPR55 antisense riboprobe. In the upper panel, arrowheads indicate neurons co-labeled with TH and GPR55 and asterisks non-dopaminergic cells labeled with the GPR55 riboprobe. An enlarged image of a dopamine neuron with the co-localization of the TH and GPR55 staining is shown in the lower panel. (C) Representative confocal images obtained from the striatum of control mice (upper panel) and MPTPp mice (lower panel). (D) Densitometry analysis of the GPR55 expression in NeuN-immunolabeled cells. (E) Real time PCR for GPR55 mRNA transcripts was performed on striatal samples from control and MPTPp mice. (F) Representative confocal images from the SNpc of control (upper panel) and MPTPp mice (lower panel). (G) Densitometry analysis of the GPR55 expression in TH-immunolabeled cells. (H) Real time PCR for GPR55 mRNA transcripts was performed in the midbrain from control and MPTPp mice. The data represent the mean $\pm$ SEM from 5 to 6 animals per group, using a Student's t-test to determine statistical differences: $*p < 40.05$, $***p < 0.001$. Scale bar: 20 μm.

3.3. The effect of GPR55 agonists in the haloperidol mouse model

To study the symptomatic effect of Abn-CBD administration in parkinsonian mice, the haloperidol mouse model was used. This model involves the antagonism of dopamine D2 receptors in medium striatal spiny neurons that comprise the indirect pathway. This animal model has been used to assess the potential symptomatic efficacy of novel non-dopaminergic anti-PD drugs, including mGlu4-positive allosteric modulators, adenosine A_{2A}/A_1 antagonists and mGlu7 agonists (Niswender et al., 2008; Neustadt
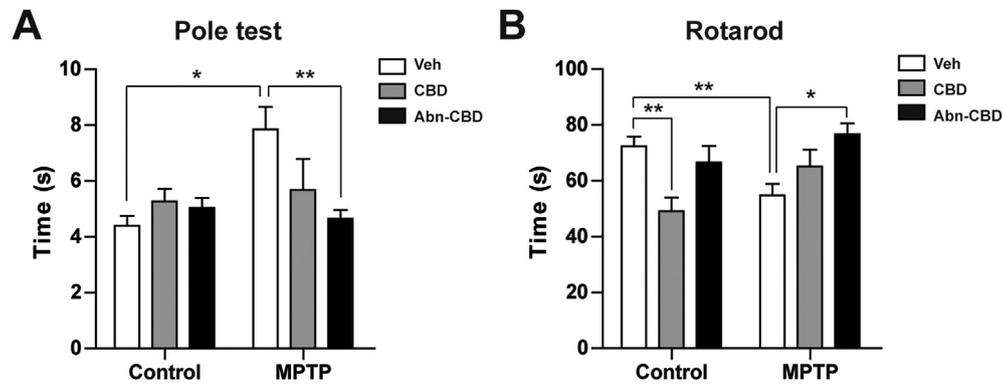
Fig. 4. Effect of CBD and Abn-CBD on motor performance in MPTPp animals. (A) In the pole test, each animal was placed facing upward on the top of a 50 cm pole and the time they took to turn around and descend the pole was recorded. (B) In the rotarod test, the animals were placed on the device and the latency until they fell was recorded as the rotarod accelerated. The data represent the mean $\pm$ SEM from 10 to 13 animals per group, and two-way ANOVA followed by a Bonferroni's multiple comparison *post-hoc* test was used to determine the statistical differences: $^*p < 0.05$, $^{**}p < 0.01$.
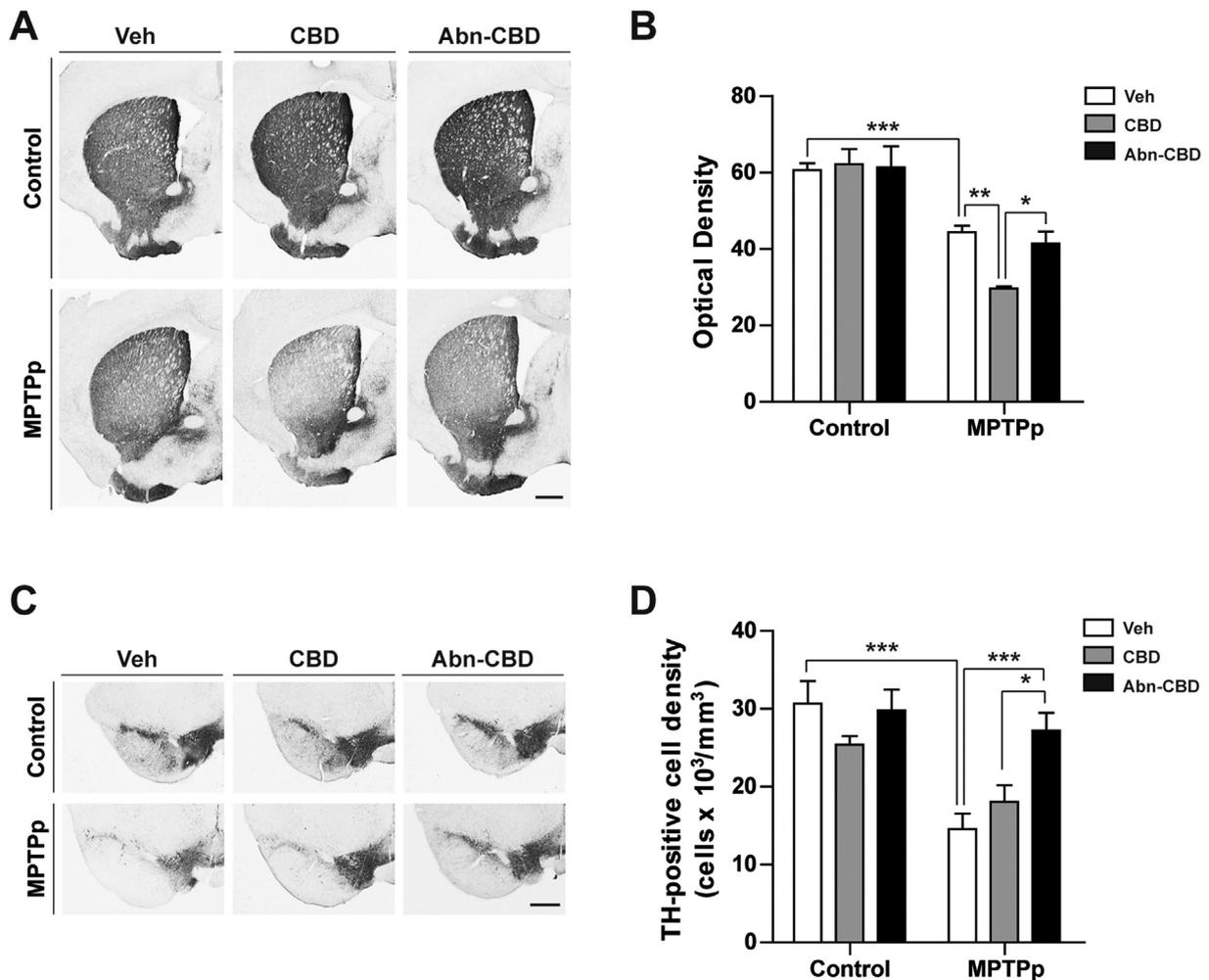

Fig. 5. Effect of chronic CBD and Abn-CBD treatment on the preservation of the nigrostriatal pathway. (A) Representative photomicrographs showing TH-immunoreactivity in the striatum. (B) Densitometry analysis of dopaminergic terminals in the striatum. (C) Representative photomicrographs showing TH-immunoreactivity in the SNpc. (D) Stereological analysis of TH-immunolabeled neurons in the SNpc. The data represent the mean $\pm$ SEM from 5 to 6 animals per group and two-way ANOVA followed by Bonferroni's multiple comparison *post-hoc* test were used to determine the statistical significance of the differences: $^*p < 0.05$, $^{**}p < 0.01$, $^{***}p < 0.001$. Scale bar: 0.5 mm.

et al., 2009; Greco et al., 2010; Shook et al., 2010). Blockage of D2 receptors results in rigidity and catalepsy in rodents, mimicking the difficulties of PD patients in the initiation of movement. Therefore, the aim was to investigate whether the antiparkinsonian effect of

Abn-CBD in the MPTP model could be replicated in haloperidol-treated animals. Two hours after haloperidol administration (1 mg/kg, i.p.) mice were injected (i.p.) with the vehicle, Abn-CBD, CBD or SCH442416 (1 mg/kg), the latter a selective adenosine A_{2A}
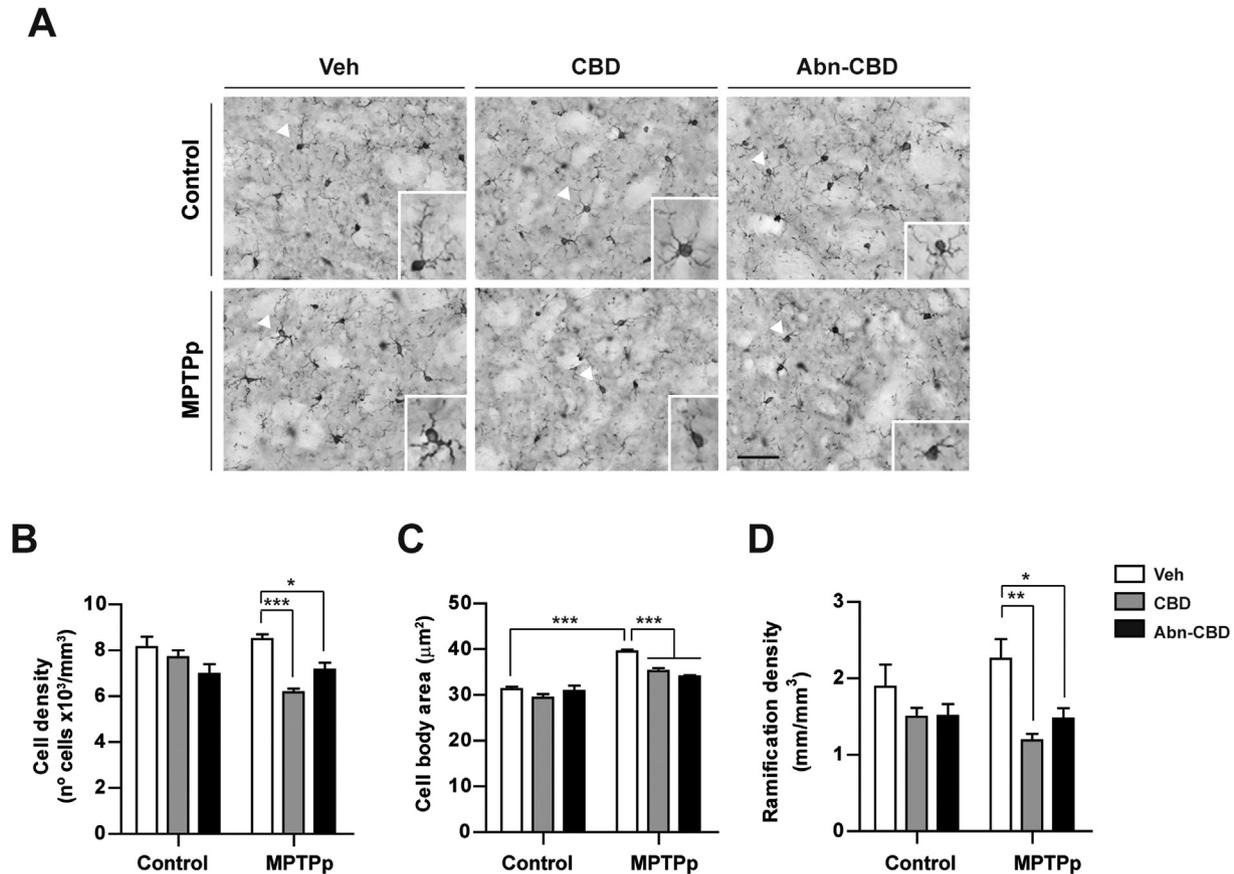
Fig. 6. Morphological analysis of Iba1-immunolabeled cells in samples from MPTPp animals treated chronically with CBD or Abn-CBD. (A) Representative photomicrographs of Iba1-immunostained microglia in the striatum, arrowheads point to the cell amplified in the insert Stereological quantification of microglial cell density (B), cell body area (C) and microglial ramification length (D). The data represent the mean ± SEM from 5 to 6 animals and these results were analyzed using two-way ANOVA followed by Bonferroni's multiple comparison *post-hoc* test to determine the statistical significance of the differences: *$p < 0.05$, **$p < 0.01$, ***$p < 0.001$. Scale bar: 50 μm.
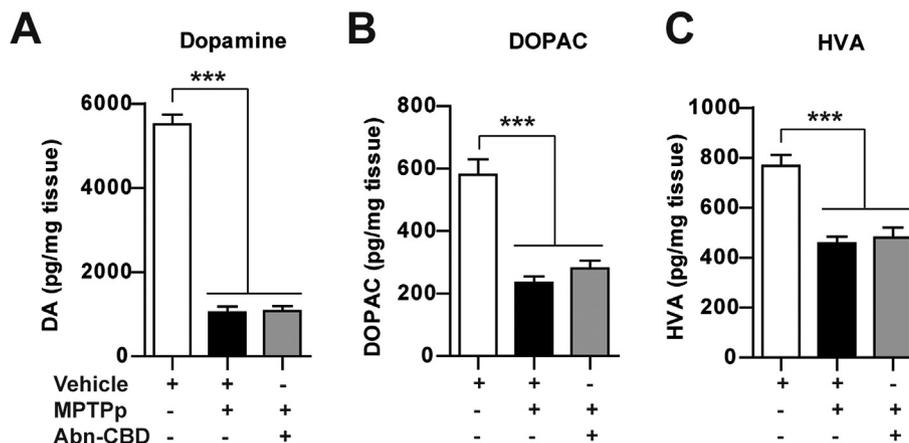
Fig. 7. Effect of chronic Abn-CBD administration on striatal levels of DA, DOPAC and HVA. Striatal content of DA (A), and its metabolites DOPAC (B) and HVA (C), were determined by HPLC in control, MPTPp and MPTPp mice treated with Abn-CBD. The data represent the mean ± SEM from 5 to 7 animals and an one-way ANOVA followed Bonferroni's multiple comparison *post-hoc* test was used to determine the statistical significance of the differences: ***$p < 0.001$.

receptor antagonist used as positive control (Fig. 8A). The cataleptic status was assessed 1 h later in the bar test, and SCH442416 and Abn-CBD (20 mg/kg) significantly decreased the time mice stayed on the bar relative to the haloperidol-treated mice that received the vehicle alone (Fig. 8B). CBD administration (5 mg/kg, Fig. 8C; 20 mg/kg, Fig. 8D) did not produce such an anti-cataleptic effect and moreover, it blocked the anti-cataleptic effect of Abn-CBD (Fig. 8D).

Furthermore, the anti-cataleptic effect of Abn-CBD was completely abolished by the GPR55 antagonist, PSB1216 (10 mg/kg, Fig. 8E) (see Supplementary data for information on antagonistic properties of PSB1216, Fig. S2), although the benefits of Abn-CBD were neither affected by a CB_1 receptor antagonist, rimonabant (3 mg/kg), a CB_2 receptor antagonist, AM630 (3 mg/kg: Fig. 8F) nor a GPR18 antagonist, CID85469571 (20 mg/kg, Fig. 8G). Administration of Abn-CBD
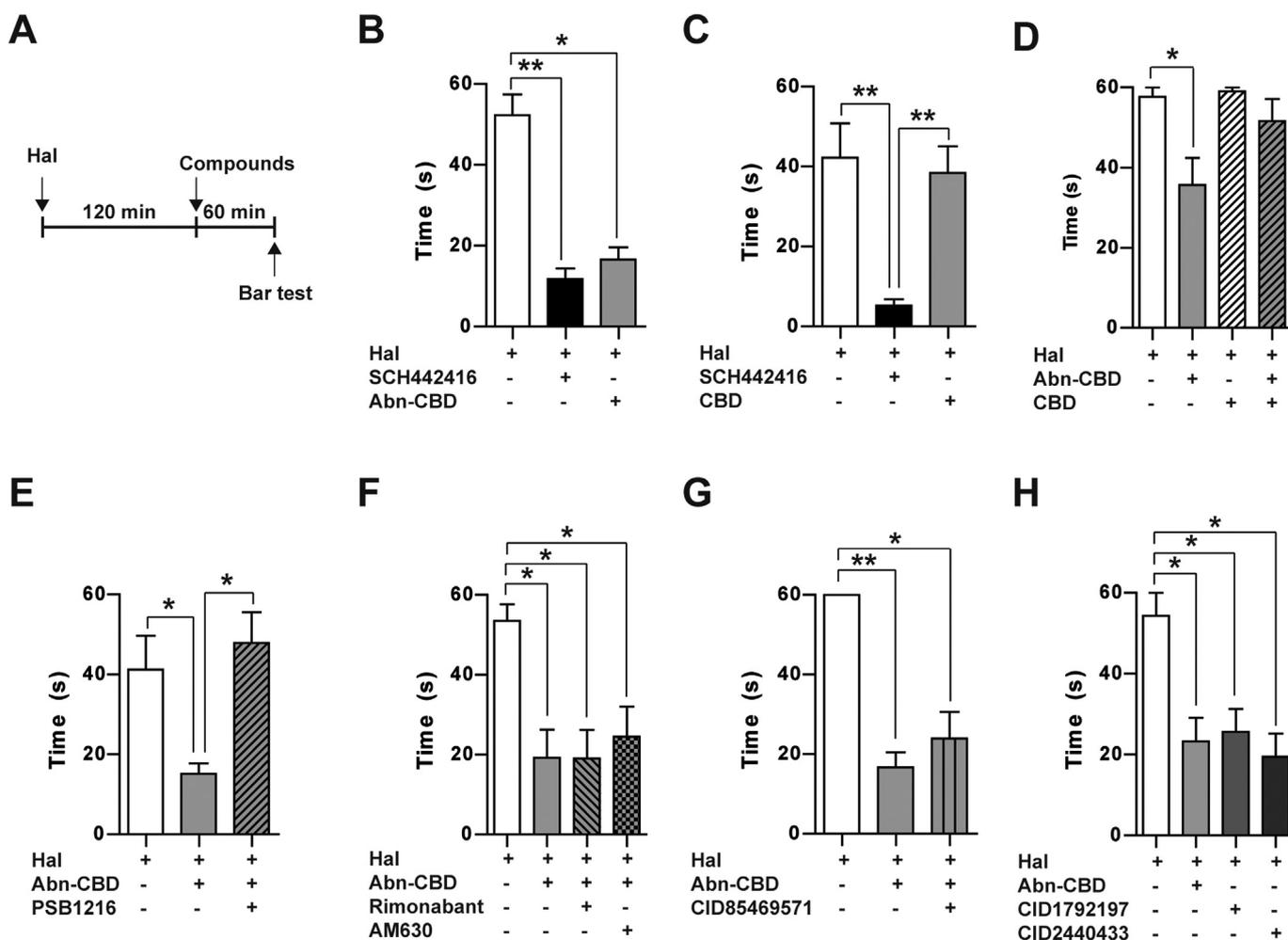
Fig. 8. Effect of CBD and Abn-CBD on haloperidol-induced catalepsy. Catalepsy was induced by the administration of haloperidol (Hal, i.p.) at a dose of 1 mg/kg. (A) Compounds were injected 120 min after the haloperidol injection and the cataleptic status was evaluated in the bar test by measuring the time each animal stayed with its forepaws standing on the bar for up to 60 s. (B) Catalepsy was measured in animals treated with SCH442416 (1 mg/kg, used as a positive control), Abn-CBD (20 mg/kg), (C) CBD (5 mg/kg) or (D) CBD (20 mg/kg). The anti-cataleptic effect of Abn-CBD was blocked by (D) CBD (20 mg/kg) and (E) the GPR55 antagonist, PSB1216 (10 mg/kg). (F) Antagonists of the CB_1 (rimonabant, 3 mg/kg), CB_2 receptor (AM630, 3 mg/kg) and (G) GPR18 (CID85469571, 20 mg/kg) did not abolish the anti-cataleptic properties of Abn-CBD. (H) Two different GPR55 agonists, CID1792197 (10 mg/kg) and CID2440433 (40 mg/kg), displayed an anti-cataleptic effect similar to that of Abn-CBD. The data were analyzed using a Kruskal-Wallis test followed by Dunn's multiple comparison *post-hoc* test to determine statistical significance of the differences (n = 6 animals per group): *$p < 0.05$, **$p < 0.01$.

(20 mg/kg) to naïve animals showed that brain penetration was almost complete at 60 min (LogBB = −0.08, values close to 0 indicate equimolar concentration in brain and plasma). Abn-CBD brain concentration was 476 nM, this concentration value is nearly 200-fold higher than that reporter by GlaxoSmithKline (GPR55, EC_{50} value of 2.5 nM; Johns et al., 2007). GPR55 may be saturated and our data would support the involvement of GPR55 in the functional response.

Finally, the anti-cataleptic properties of two different chemical GPR55 agonists were assayed, CID1792197 and CID2440433. The permeability of both these compounds was studied first taking into account the permeability values determined for known commercial drugs with either high or low brain penetration (Di et al., 2003). The values were corrected based on the internal permeability values obtained in our *in-vitro* assay relative to the known *in-vivo* brain permeation (Rabal et al., 2016; Sánchez-Arias et al., 2016). The ranges to classify cell permeation are: poor (Pe < 10 nm/s), moderate (10 < Pe < 30 nm/s), and good (Pe > 30 nm/s). The two GPR55 agonists, CID1792197 and CID2440433, showed low (Pe = 1.3 nm/s) and good (Pe = 68.1 nm/s) permeability, respectively. *In-vivo*,

CID1792197 (10 mg/kg) and CID2440433 (10 mg/kg) were administered i.p. to mice that had received haloperidol. Both compounds exerted anti-cataleptic properties similar to those of Abn-CBD (Fig. 8H). Hence, these results indicate that GPR55 activation reverses the haloperidol-induced catalepsy in a similar manner to other compounds with known anti-parkinsonian properties, such as A_{2A} receptor antagonists.

Cannabinoids that act via CB_1 and/or CB_2 receptors have long been associated with four well characterized behaviors in rodents, known as the cannabinoid tetrad: hypothermia, anti-nociception, hypolocomotion, and catalepsy (Little et al., 1988; Wiley et al., 2014). In fact, all these symptoms were observed when animals were administered the non-selective CB_1/CB_2 receptor agonist WIN55,212-2 (3 mg/kg). This compound significantly reduced body temperature (Fig. S2A), it had an analgesic effect in the tail-flick test (Fig. S2B), it induced catalepsy in mice (Fig. S2C) and it significantly decreased locomotor activity in the open field test (Fig. S2D). When the same tests were performed on animals treated with Abn-CBD or CBD for 7 days, none of these symptoms were detected up to 1 h after the last administration (Figs. S2A, S2B, S2C, S2D).

4. Discussion

The absence of potent, rigorously validated, specific GPR55 agonists and antagonists makes it very challenging to use a pharmacological approach to determine the endogenous functions of this receptor and its relationship with disease. In this study, Abn-CBD was selected as an agonist of GPR55 activity to address whether modulation of GPR55 might be of interest to treat PD. We first assessed the expression of this receptor in the brain areas affected in this neurodegenerative disease. Then, we explored the effect of the synthetic isomer of CBD, Abn-CBD, in the chronic MPTPp mouse model. Abn-CBD induced a significant improvement in motor behavior that was not observed in MPTP animals that received CBD instead of Abn-CBD. Although Abn-CBD exerted a clear neuroprotective effect on dopaminergic cell bodies, it failed to prevent degeneration of the dopaminergic terminals in the striatum, indicating that preservation of the nigrostriatal pathway could not explain the improvement in motor behavior. Finally, a catalepsy test was used to study the symptomatic effect of Abn-CBD and two other GPR55 agonists indicating that GPR55 could be a potential symptomatic therapeutic target for the treatment of PD.

The expression of GPR55 in mouse tissue has been described by quantitative PCR, showing a broad distribution in the nervous system that includes the frontal cortex, striatum, hippocampus and cerebellum (Ryberg et al., 2007; Wu et al., 2013). Northern blot analysis in human brain tissues demonstrated the presence of GPR55 mRNA in the caudate and putamen, while there was no evidence of GPR55 transcripts in the frontal cortex, pons, hippocampus, thalamus or cerebellum (Sawzdargo et al., 1999). GPR55 mRNA is expressed in primary cultures of mouse microglia cells and by a murine microglial cell line, and its expression is regulated by LPS or INFγ (Pietr et al., 2009). Activation of microglial GPR55 with LPI exerts a neuroprotective activity on organotypic hippocampal slice cultures (Kallendrusch et al., 2013).

The use of *in situ* hybridization to detect GPR55 transcripts confirmed the expression of GPR55 in the mice striatum, cortex and hippocampus described previously, and these studies provided additional evidence for its presence in the GPe, STN and SN. Furthermore, GPR55 transcripts co-localized with the neuronal marker NeuN, whereas no expression was detected in astroglia or microglia in the striatum or midbrain. The higher sensitivity of PCR compared to Northern blotting or ISH to detect GPR55 transcripts, and the different nature of samples (cell cultures vs brain tissue) may account for these differences. The expression of GPR55 was profoundly downregulated in the striatum of the mouse PD models, suggesting that GPR55 might be involved in the pathology of this disease. However, downregulation of GPR55 expression in the midbrain seemed to be related to the loss of dopaminergic neurons, since no changes in GPR55 expression were detected in the remaining SNpc neurons.

Modulation of the cannabinoid system has been reported to exert anti-parkinsonian properties through different mechanisms. On one hand, cannabinoids have neuroprotective properties in different rodent models of PD, both through a CB_1/CB_2 receptor-independent mechanism (Lastres-Becker et al., 2005) and by modulating glial cell activity in a manner that involves CB_2 receptors (Price et al., 2009; Fernández-Suárez et al., 2014; Aymerich et al., 2016). On the other hand, pharmacological modulation of the endocannabinoid anandamide (AEA) showed promise in terms of the symptomatic treatment of the disease (Kreitzer and Malenka, 2007; More and Choi, 2015; Celorrio et al., 2016). In this study, we questioned whether modulating GPR55 could have anti-parkinsonian effects, either neuroprotective or symptomatic. CBD was proposed to have a neuroprotective action in the 6-OHDA rat model through a CB_1/CB_2 receptor-independent mechanism,

probably due to its antioxidant properties (Lastres-Becker et al., 2005; García-arencibia et al., 2006). By contrast, we found that CBD lacked neuroprotective activity in the MPTP mouse model and it even exacerbated the effect of MPTP by increasing the loss of dopaminergic terminals in the striatum. CBD also worsened the performance of control animals in the rotarod test. MPTP and 6-OHDA are the most widely used neurotoxins to induce a nigrostriatal lesion in animal models: 6-OHDA causes massive oxidative stress and respiratory inhibition due to free radical formation; MPTP impairs mitochondrial respiration by inhibiting complex I of the electron transport chain (Schober, 2004). The different type of cell death induced by these two neurotoxins, the acute administration of 6-OHDA compared to the chronic administration of MPTP, and the different techniques used to evaluate the preservation of the nigrostriatal pathway (TH mRNA and activity *vs* stereology) might account for the differences observed in these models. Thus, caution must be taken when proposing CBD as a neuroprotective agent since the specific type of cell death might determine the beneficial or deleterious properties of this compound. Although Ryberg et al. showed results consistent with antagonism of GPR55 (Ryberg et al., 2007), CBD exerts effects via serotonin 1A (Russo et al., 2005) and cannabinoid (see McPartland et al., 2015 for review) receptors, and it has been reported as allosteric modulator of CB_1 receptors (Laprairie et al., 2015). Therefore, CBD effects *in-vivo* may result from a combination of actions in overlapping regulatory systems.

Our data show that the improvement in motor behavior in animals treated with Abn-CBD could not be explained by the preservation of the nigrostriatal pathway or by a compensatory effect in DA metabolism. The strong expression of GPR55 in the basal ganglia led us to explore the possibility that Abn-CBD might act through these receptors to induce symptomatic relief from the motor symptoms. Using the haloperidol-induced catalepsy mouse model, Abn-CBD exhibited a clear anti-cataleptic effect that was reversed by GPR55 antagonists but not by antagonists of CB_1, CB_2 or GPR18 receptors. Two agonists of GPR55 with a different chemical structure to that of Abn-CBD also had anti-cataleptic properties. The mechanism of action to induce a motor deficit in the chronic MPTP mouse model and in the haloperidol-induced catalepsy model is different. In the chronic MPTP mouse model, MPTP is administered twice a week with probenecid, which reduces the renal clearance of MPTP leading to a sustained toxic response that result in dopaminergic neuron loss and a permanent decrease in striatal dopamine levels. We considered that the behavior analyzed at 16 h after the last dose of Abn-CBD (24 h after MPTPp) would still be under the influence of MPTP and the Abn-CBD. In fact, animals treated with MPTP and Abn-CBD showed a motor behavior clearly different from animals receiving only MPTP, which indicates that at 16 h after the last dose the effect of Abn-CBD was still detectable. The haloperidol-induced catalepsy mouse model is a transient model. Haloperidol is an antagonist of D_2 receptors, but it does not affect striatal dopamine levels. The results obtained using these two different models are consistent with Abn-CBD improving PD-related motor deficits. Furthermore, a careful analysis of motor behavior in two independent GPR55 deficient mice provided clear evidence that GPR55 has a subtle but defined modulatory influence on motor control (Wu et al., 2013; Meadows et al., 2015; Bjursell et al., 2016), consistent with the expression of GPR55 in brain areas important to motor function. Together, these results indicate that GPR55 is involved in the anti-parkinsonian properties of Abn-CBD, constituting the first evidence that GPR55 could be considered as a therapeutic target for PD.

Abn-CBD induced changes (reduced microglial cell density, cell body size and a lower density of ramification) in the microglial morphology that could be compatible with a blockade of the

neuroinflammation provoked by MPTPp. The absence of GPR55 transcripts in microglial cells in striatum and the similar effect of both drugs on microglia suggest that this effect might be independent of the GPR55 activation in the brain. Furthermore, these changes do not correlate with the degree of dopaminergic degeneration. Using a similar experimental approach, we identified a neuroprotective microglial phenotype in MPTPp mice treated with a monoacylglycerol lipase inhibitor, the main morphological characteristic of these cells being the abundance of large and thin ramifications (Fernández-Suárez et al., 2014). The specific modulation of microglial morphology seems to reflect the different microglial activation states that exert a distinct effect in terms of neuroprotection.

In this study, for the first time we propose GPR55 as a therapeutic target for the treatment of PD. GPR55 expression is abundant in neurons located in brain nuclei related to the control of movement in mice. Abn-CBD has a symptomatic effect in parkinsonian mice that is mediated by GPR55. Together, our findings indicate that GPR55 activation might be a therapeutic target for the non-dopaminergic symptomatic treatment of PD.

Acknowledgements

Appendix A. Supplementary data

Supplementary data related to this article can be found at http://dx.doi.org/10.1016/j.neuropharm.2017.08.017.

References

Aymerich, M.S., Rojo-Bustamante, E., Molina, C., Celorrio, M., Sánchez-Arias, J.A., Franco, R., 2016. Neuroprotective effect of JZL184 in MPP+–treated SH-SY5Y cells through CB2 receptors. Mol. Neurobiol. 53, 2312–2319. http://dx.doi.org/10.1007/s12035-015-9213-3.

Baker, D., Pryce, G., Davies, W.L., Hiley, C.R., 2006. In silico patent searching reveals a new cannabinoid receptor. Trends Pharmacol. Sci. http://dx.doi.org/10.1016/j.tips.2005.11.003.

Bjursell, M., Ryberg, E., Wu, T., Greasley, P.J., Bohlooly, Y.,M., Hjorth, S., 2016. Deletion of Gpr55 results in subtle effects on energy metabolism, motor activity and thermal pain sensation. PLoS One 11, e0167965. http://dx.doi.org/10.1371/journal.pone.0167965.

Carroll, C.B., Bain, P.G., Teare, L., Bch, B.M., Liu, X., Joint, C., Wroath, C., Parkin, S.G., Bch, B.M., Fox, P., Bch, B.M., Wright, D., Hobart, J., Zajicek, J.P., 2004. Cannabis for dyskinesia in Parkinson disease A randomized double-blind crossover study. Neurology 63, 1245–1250. http://dx.doi.org/10.1212/01.WNL.0000140288.48796.8E.

Celorrio, M., Fernández-Suárez, D., Rojo-Bustamante, E., Echeverry-Alzate, V., Ramírez, M.J., Hillard, C.J., López-Moreno, J.A., Maldonado, R., Oyarzábal, J., Franco, R., Aymerich, M.S., 2016. Fatty acid amide hydrolase inhibition for the symptomatic relief of Parkinson's disease. Brain. Behav. Immun. 57, 94–105. http://dx.doi.org/10.1016/j.bbi.2016.06.010.

Cherif, H., Argaw, A., Cécyre, B., Bouchard, A., Gagnon, J., Javadi, P., Desgent, S., Mackie, K., Bouchard, J.-F., 2015. Role of GPR55 during axon growth and target innervation. eNeuro 2. http://dx.doi.org/10.1523/ENEURO.0011-15.2015.

Di, L., Kerns, E.H., Fan, K., McConnell, O.J., Carter, G.T., 2003. High throughput artificial membrane permeability assay for blood-brain barrier. Eur. J. Med. Chem. 38, 223–232.

Drøjdahl, N., Nielsen, H.H., Gardi, J.E., Wree, A., Peterson, A.C., Nyengaard, J.R., Eyer, J., Finsen, B., 2010. Axonal plasticity elicits long-term changes in oligodendroglia and myelinated fibers. Glia 58, 29–42. http://dx.doi.org/10.1002/glia.20897.

Esposito, G., Scuderi, C., Savani, C., Steardo, L., De Filippis, D., Cottone, P., Iuvone, T., Cuomo, V., 2007. Cannabidiol in vivo blunts beta-amyloid induced neuroinflammation by suppressing IL-1beta and iNOS expression. Br. J. Pharmacol.

151, 1272–1279. http://dx.doi.org/10.1038/sj.bjp.0707337.

Fernández-Suárez, D., Celorrio, M., Riezu-Boj, J.I., Ugarte, A., Pacheco, R., González, H., Oyarzabal, J., Hillard, C.J., Franco, R., Aymerich, M.S., 2014. Monoacylglycerol lipase inhibitor JZL184 is neuroprotective and alters glial cell phenotype in the chronic MPTP mouse model. Neurobiol. Aging 35, 2603–2616. http://dx.doi.org/10.1016/j.neurobiolaging.2014.05.021.

García-arencibia, M., González, S., Lago, E. De, Ramos, J.A., Mechoulam, R., Fernández-ruiz, J., 2006. Evaluation of the neuroprotective effect of cannabinoids in a rat model of Parkinson â€™ s disease: importance of antioxidant and cannabinoid receptor-independent properties. Brain Res. 1134, 162–170. http://dx.doi.org/10.1016/j.brainres.2006.11.063.

Goñi-Allo, B., Ramos, M., Herv'as, I., Lasheras, B., Aguirre, N., 2006. Studies on striatal neurotoxicity caused by the 3,4-methylenedioxymethamphetamine/malonate combination: implications for serotonin/dopamine interactions. J. Psychopharmacol. 20, 245–256. http://dx.doi.org/10.1177/0269881106063264.

Greco, B., Lopez, S., van der Putten, H., Flor, P.J., Amalric, M., 2010. Metabotropic glutamate 7 receptor subtype modulates motor symptoms in rodent models of Parkinson's disease. J. Pharmacol. Exp. Ther. 332, 1064–1071. http://dx.doi.org/10.1124/jpet.109.162115.

Gundersen, H.J., Jensen, E.B., 1987. The efficiency of systematic sampling in stereology and its prediction. J. Microsc. 147, 229–263.

Henstridge, C.M., Balenga, N.A.B., Kargl, J., Andradas, C., Brown, A.J., Irving, A., Sanchez, C., Waldhoer, M., 2011. Minireview: recent developments in the physiology and pathology of the lysophosphatidylinositol-sensitive receptor GPR55. Mol. Endocrinol. 25, 1835–1848. http://dx.doi.org/10.1210/me.2011-1197.

Henstridge, C.M., Balenga, N. a B., Ford, L. a, Ross, R. a, Waldhoer, M., Irving, A.J., 2009. The GPR55 ligand L-alpha-lysophosphatidylinositol promotes RhoA-dependent Ca2+ signaling and NFAT activation. FASEB J. 23, 183–193. http://dx.doi.org/10.1096/fj.08-108670.

Iuvone, T., Esposito, G., De Filippis, D., Scuderi, C., Steardo, L., 2009. Cannabidiol: a promising drug for neurodegenerative disorders? CNS Neurosci. Ther. 15, 65–75. http://dx.doi.org/10.1111/j.1755-5949.2008.00065.x.

Johns, D.G., Behm, D.J., Walker, D.J., Ao, Z., Shapland, E.M., Daniels, D.A., Riddick, M., Dowell, S., Staton, P.C., Green, P., Shabon, U., Bao, W., Aiyar, N., Yue, T.-L., Brown, A.J., Morrison, A.D., Douglas, S.A., 2007. The novel endocannabinoid receptor GPR55 is activated by atypical cannabinoids but does not mediate their vasodilator effects. Br. J. Pharmacol. 152, 825–831. http://dx.doi.org/10.1038/sj.bjp.0707419.

Kallendrusch, S., Kremzow, S., Nowicki, M., Grabiec, U., Winkelmann, R., Benz, A., Kraft, R., Bechmann, I., Dehghani, F., Koch, M., 2013. The G protein-coupled receptor 55 ligand l -α-Lysophosphatidylinositol exerts microglia-dependent neuroprotection after excitotoxic lesion. Glia 61, 1822–1831. http://dx.doi.org/10.1002/glia.22560.

Kreitzer, A.C., Malenka, R.C., 2007. Endocannabinoid-mediated rescue of striatal LTD and motor deficits in Parkinson's disease models. Nature 445, 643–647. http://dx.doi.org/10.1038/nature05506.

Krohn, R.M., Parsons, S.A., Fichna, J., Patel, K.D., Yates, R.M., Sharkey, K.A., Storr, M.A., 2016. Abnormal cannabidiol attenuates experimental colitis in mice, promotes wound healing and inhibits neutrophil recruitment. J. Inflamm. 13, 21. http://dx.doi.org/10.1186/s12950-016-0129-0.

Laprairie, R.B., Bagher, A.M., Kelly, M.E.M., Denovan-Wright, E.M., 2015. Cannabidiol is a negative allosteric modulator of the cannabinoid CB1 receptor. Br. J. Pharmacol. 172, 4790–4805. http://dx.doi.org/10.1111/bph.13250.

Larsen, J.O., Gundersen, H.J.G., Nielsen, J., 1998. Global spatial sampling with isotropic virtual planes: estimators of length density and total length in thick, arbitrarily orientated sections. J. Microsc. 191, 238–248. http://dx.doi.org/10.1046/j.1365-2818.1998.00365.x.

Lastres-Becker, I., Molina-Holgado, F., Ramos, J.A., Mechoulam, R., Fernandez-Ruiz, J., 2005. Cannabinoids provide neuroprotection against 6-hydroxydopamine toxicity in vivo and in vitro: relevance to Parkinson's disease. Neurobiol. Dis. 19, 96–107 doi:S0969-9961(04)00282-7 [pii]10.1016/j.nbd.2004.11.009.

Lau, Y.S., Trobough, K.L., Crampton, J.M., Wilson, J.A., 1990. Effects of probenecid on striatal dopamine depletion in acute and long-term 1-methyl-4-phenyl-1,2,3,6-tetrahydropyridine (MPTP)-treated mice. Gen. Pharmacol. 21, 181–187.

Lauckner, J.E., Jensen, J.B., Chen, H.-Y., Lu, H.-C., Hille, B., Mackie, K., 2008. GPR55 is a cannabinoid receptor that increases intracellular calcium and inhibits M current. Proc. Natl. Acad. Sci. U. S. A. 105, 2699–2704. http://dx.doi.org/10.1073/pnas.0711278105.

Little, P.J., Compton, D.R., Johnson, M.R., Melvin, L.S., Martin, B.R., 1988. Pharmacology and stereoselectivity of structurally novel cannabinoids in mice. J. Pharmacol. Exp. Ther. 247, 1046–1051.

Marichal-Cancino, B.A., Sánchez-Fuentes, A., Méndez-Díaz, M., Ruiz-Contreras, A.E., Prospéro-García, O., 2016. Blockade of GPR55 in the dorsolateral striatum impairs performance of rats in a T-maze paradigm. Behav. Pharmacol. 27, 393–396. http://dx.doi.org/10.1097/FBP.0000000000000185.

McKillop, A.M., Moran, B.M., Abdel-Wahab, Y.H.A., Flatt, P.R., 2013. Evaluation of the insulin releasing and antihyperglycaemic activities of GPR55 lipid agonists using clonal beta-cells, isolated pancreatic islets and mice. Br. J. Pharmacol. 170, 978–990. http://dx.doi.org/10.1111/bph.12356.

McKillop, A.M., Moran, B.M., Abdel-Wahab, Y.H.A., Gormley, N.M., Flatt, P.R., 2016. Metabolic effects of orally administered small-molecule agonists of GPR55 and GPR119 in multiple low-dose streptozotocin-induced diabetic and incretin-

receptor-knockout mice. Diabetologia. http://dx.doi.org/10.1007/s00125-016-4108-z.

McPartland, J.M., Duncan, M., Di Marzo, V., Pertwee, R.G., 2015. Are cannabidiol and ??9-tetrahydrocannabivarin negative modulators of the endocannabinoid system? A systematic review. Br. J. Pharmacol. 172, 737–753. http://dx.doi.org/10.1111/bph.12944.

Meadows, A., Lee, J., Wu, C.-S., Wei, Q., Pradhan, G., Yafi, M., Lu, H.-C., Sun, Y., 2015. Deletion of G-protein-coupled receptor 55 promotes obesity by reducing physical activity. Int. J. Obes. 40, 417–424. http://dx.doi.org/10.1038/ijo.2015.209.

More, S.V., Choi, D.-K., 2015. Promising cannabinoid-based therapies for Parkinson's disease: motor symptoms to neuroprotection. Mol. Neurodegener. 10, 17. http://dx.doi.org/10.1186/s13024-015-0012-0.

Neustadt, B.R., Liu, H., Hao, J., Greenlee, W.J., Stamford, A.W., Foster, C., Arik, L., Lachowicz, J., Zhang, H., Bertorelli, R., Fredduzzi, S., Varty, G., Cohen-Williams, M., Ng, K., 2009. Potent and selective adenosine A2A receptor antagonists: 1,2,4-Triazolo[1,5-c]pyrimidines. Bioorg. Med. Chem. Lett. 19, 967–971. http://dx.doi.org/10.1016/j.bmcl.2008.11.075.

Niswender, C.M., Johnson, K.A., Weaver, C.D., Jones, C.K., Xiang, Z., Luo, Q., Rodriguez, A.L., Marlo, J.E., de Paulis, T., Thompson, A.D., Days, E.L., Nalywajko, T., Austin, C.A., Williams, M.B., Ayala, J.E., Williams, R., Lindsley, C.W., Conn, P.J., 2008. Discovery, characterization, and antiparkinsonian effect of novel positive allosteric modulators of metabotropic glutamate receptor 4. Mol. Pharmacol. 74, 1345–1358. http://dx.doi.org/10.1124/mol.108.049551.

Oka, S., Nakajima, K., Yamashita, A., Kishimoto, S., Sugiura, T., 2007. Identification of GPR55 as a Lysophosphatidylinositol Receptor. http://dx.doi.org/10.1016/j.bbrc.2007.08.078.

Paxinos, G., Franklin, K.B., 2001. The Mouse Brain in Sterotaxic Coordinates. Academic Press.

Petitet, F., Donlan, M., Michel, A., 2006. GPR55 as a new cannabinoid receptor: still a long way to prove it. Chem. Biol. Drug Des. http://dx.doi.org/10.1111/j.1747-0285.2006.00370.x.

Petroske, E., Meredith, G.E., Callen, S., Totterdell, S., Lau, Y.S., 2001. Mouse model of Parkinsonism: a comparison between subacute MPTP and chronic MPTP/probenecid treatment. Neuroscience 106, 589–601 doi:S0306-4522(01)00295-0 [pii].

Pietr, M., Kozela, E., Levy, R., Rimmerman, N., Lin, Y.H., Stella, N., Vogel, Z., Juknat, A., 2009. Differential changes in GPR55 during microglial cell activation. FEBS Lett. 583, 2071–2076. http://dx.doi.org/10.1016/j.febslet.2009.05.028.

Price, D.A., Martinez, A.A., Seillier, A., Koek, W., Acosta, Y., Fernandez, E., Strong, R., Lutz, B., Marsicano, G., Roberts, J.L., Giuffrida, A., 2009. WIN55,212-2, a cannabinoid receptor agonist, protects against nigrostriatal cell loss in the 1-methyl-4-phenyl-1,2,3,6-tetrahydropyridine mouse model of Parkinson's disease. Eur. J. Neurosci. 29, 2177–2186. http://dx.doi.org/10.1111/j.1460-9568.2009.06764.x.

Rabal, O., Sánchez-Arias, J.A., Cuadrado-Tejedor, M., de Miguel, I., Pérez-González, M., García-Barroso, C., Ugarte, A., Estella-Hermoso de Mendoza, A., Sáez, E., Espelosin, M., Ursua, S., Haizhong, T., Wei, W., Musheng, X., Garcia-Osta, A., Oyarzabal, J., 2016. Design, synthesis, and biological evaluation of first-in-class dual acting histone deacetylases (HDACs) and phosphodiesterase 5 (PDE5) inhibitors for the treatment of Alzheimer's disease. J. Med. Chem. 59, 8967–9004. http://dx.doi.org/10.1021/acs.jmedchem.6b00908.

Ross, R.A., 2009. The enigmatic pharmacology of GPR55. Trends Pharmacol. Sci. 30, 156–163. http://dx.doi.org/10.1016/j.tips.2008.12.004.

Russo, E.B., Burnett, A., Hall, B., Parker, K.K., 2005. Agonistic properties of cannabidiol at 5-HT1a receptors. Neurochem. Res. 30, 1037–1043. http://dx.doi.org/10.1007/s11064-005-6978-1.

Ryberg, E., Larsson, N., Sjögren, S., Hjorth, S., Hermansson, N.-O., Leonova, J., Elebring, T., Nilsson, K., Drmota, T., Greasley, P.J., 2007. The orphan receptor GPR55 is a novel cannabinoid receptor. Br. J. Pharmacol. 152, 1092–1101. http://dx.doi.org/10.1038/sj.bjp.0707460.

Sánchez-Arias, J.A., Rabal, O., Cuadrado-Tejedor, M., de Miguel, I., Pérez-González, M., Ugarte, A., Sáez, E., Espelosin, M., Ursua, S., Haizhong, T., Wei, W., Musheng, X., Garcia-Osta, A., Oyarzabal, J., 2016. Impact of scaffold exploration on novel dual-acting histone deacetylases and phosphodiesterase 5 inhibitors for the treatment of Alzheimer's disease. ACS Chem. Neurosci. 6b00370. http://dx.doi.org/10.1021/acschemneuro.6b00370.

Sawzdargo, M., Nguyen, T., Lee, D.K., Lynch, K.R., Cheng, R., Heng, H.H.Q., George, S.R., O'Dowd, B.F., 1999. Identification and cloning of three novel human G protein-coupled receptor genes GPR52, ΨGPR53 and GPR55: GPR55 is extensively expressed in human brain. Mol. Brain Res. 64, 193–198. http://dx.doi.org/10.1016/S0169-328X(98)00277-0.

Schicho, R., Bashashati, M., Bawa, M., McHugh, D., Saur, D., Hu, H.M., Zimmer, A., Lutz, B., MacKie, K., Bradshaw, H.B., McCafferty, D.M., Sharkey, K.A., Storr, M., 2011. The atypical cannabinoid O-1602 protects against experimental colitis and inhibits neutrophil recruitment. Inflamm. Bowel Dis. 17, 1651–1664. http://dx.doi.org/10.1002/ibd.21538.

Schober, A., 2004. Classic toxin-induced animal models of Parkinson's disease: 6-OHDA and MPTP. Cell Tissue Res. 318, 215–224. http://dx.doi.org/10.1007/s00441-004-0938-y.

Shook, B.C., Rassnick, S., Osborne, M.C., Davis, S., Westover, L., Boulet, J., Hall, D., Rupert, K.C., Heintzelman, G.R., Hansen, K., Chakravarty, D., Bullington, J.L., Russell, R., Branum, S., Wells, K.M., Damon, S., Youells, S., Li, X., Beauchamp, D.A., Palmer, D., Reyes, M., Demarest, K., Tang, Y., Rhodes, K., Jackson, P.F., 2010. In vivo characterization of a dual adenosine A2A/A1 receptor antagonist in animal models of Parkinson's disease. J. Med. Chem. 53, 8104–8115. http://dx.doi.org/10.1021/jm100971t.

Staton, P.C., Hatcher, J.P., Walker, D.J., Morrison, A.D., Shapland, E.M., Hughes, J.P., Chong, E., Mander, P.K., Green, P.J., Billinton, A., Fulleylove, M., Lancaster, H.C., Smith, J.C., Bailey, L.T., Wise, A., Brown, A.J., Richardson, J.C., Chessell, I.P., 2008. The putative cannabinoid receptor GPR55 plays a role in mechanical hyperalgesia associated with inflammatory and neuropathic pain. Pain 139, 225–236. http://dx.doi.org/10.1016/j.pain.2008.04.006.

Su, E.N., Kelly, M.E., Cringle, S.J., Yu, D.Y., 2015. Role of endothelium in abnormal cannabidiol-induced vasoactivity in retinal arterioles. Investig. Ophthalmol. Vis. Sci. 56, 4029–4037. http://dx.doi.org/10.1167/iovs.14-14879.

Wiley, J.L., Marusich, J.A., Huffman, J.W., 2014. Moving around the molecule: relationship between chemical structure and in vivo activity of synthetic cannabinoids. Life Sci. 97, 55–63. http://dx.doi.org/10.1016/j.lfs.2013.09.011.

Wu, C.S., Chen, H., Sun, H., Zhu, J., Jew, C.P., Wager-Miller, J., Straiker, A., Spencer, C., Bradshaw, H., Mackie, K., Lu, H.C., 2013. GPR55, a G-protein coupled receptor for lysophosphatidylinositol, plays a role in motor coordination. PLoS One 8, e60314. http://dx.doi.org/10.1371/journal.pone.0060314PONE-D-12-30016 [pii].